

DEVELOPMENT OF A WEARABLE GLOVE USING SOFT FINGER ACTUATORS FOR MEDICAL REHABILITATION

Nhu Thanh Vo¹, Hoai Nam Le^{1*}, Thi Tran Ha Bao¹, Viet Nguyen Huu¹, Chinh Le Nhat¹, Anh-Duc Pham¹
¹Faculty of Mechanical Engineering, The University of Danang – University of Science and Technology, 54 Nguyen Luong Bang, Lien Chieu, Danang, Vietnam
Email: lehoainam@dut.udn.vn

Abstract - Stroke patients can benefit significantly from active recovery during the critical "golden period" following a cerebrovascular event. While healthcare professionals provide support, self-directed training is also crucial for rehabilitation. This paper presents the structural design of bidirectional soft pneumatic actuators, the fabrication process, and the implementation of a soft rehabilitation wearable glove. Finite Element Analysis (FEA) simulations and experiments were performed to evaluate the mechanical behaviour and performance of the glove, specifically with respect to bending angle and force outputs during pressurization. The glove operation was controlled via a Peripheral Interface Controller (PIC) microcontroller-based hardware system. The actuators between each finger provided extension and contraction motions, enhancing the effectiveness of rehabilitation. Experimental evaluations focused on rehabilitation training at a clinic center with real patients. The results from the experiments indicate that the developed device has the potential to significantly improve hand mobility and increase the range of training.

Keywords: Rehabilitation glove, Soft robotics, Stroke rehabilitation, Soft pneumatic actuator.

1. Introduction

Stroke is a major cause of mortality and disability worldwide, affecting approximately 15 million people annually [1]. In Vietnam, the stroke rate is among the highest in the world, at 576 per 100,000 people [2]. Stroke patients face numerous challenges, including limited access to healthcare facilities and rehabilitation equipment.

Research on hand rehabilitation devices for stroke patients has focused primarily on rigid hand exoskeletons [3-5] and soft assistive gloves [6-8]. Traditional rigid robots, driven by electric motors, often have complex mechanisms and significant weights, which can cause discomfort and potential risks for patients. In contrast, soft wearable rehabilitation gloves, which are made from soft materials and typically powered by cables, smart materials, or pneumatic/hydraulic actuators, provide a jointless structure that is comfortable and safer for users. Owing to their lightweight nature, portability, high power to weight ratio, affordability, and excellent human-machine interaction, soft wearable gloves are considered more promising for hand rehabilitation than rigid alternatives are. These gloves have the potential to enhance rehabilitation, lower patient costs, and expedite recovery, allowing individuals to reintegrate into family and society more quickly.

Inspired by bionic designs, soft joints based on composite fabric materials have been introduced for soft glove development [8]. Lightweight gloves capable of extension and contraction can be produced via 3D printing technology [9], whereas deep learning techniques can be employed for position estimation and control [10]. Additionally, force feedback gloves have been proposed to generate haptic signals, improving control in remote or virtual tasks [11].

Soft robot actuators generally utilize pneumatic/hydraulic drives [12] and cable/tendon drives [13]. Pneumatic- or hydraulic-actuated gloves are typically made with polymers or fabrics that form embedded chambers, which enable bending and extension motions when pressurized. Various soft gloves for hand rehabilitation have been developed in recent years. Elastomeric chambers reinforced by fibres were designed to produce bending, twisting, and extending motions [14]. A soft robotic glove using fabric materials was created to assist hand impaired patients, offering bidirectional finger flexion and extension [15]. A high-force fabric-based pneumatic actuator with asymmetric chambers and interference pads was developed, which improved the stiffness and output force [16]. A fabric-based glove was designed to assist hand opening and closing, and a circular finger stretching mechanism was introduced for rehabilitation [17]. A circular finger stretching mechanism inspired by the extensor tendon for hand rehabilitation was

developed via a biomimetic approach [18]. Additionally, a glove with a nondeformable rod for bone support was designed and fabricated [19].

Among various soft robotic technologies, Pneumatic Networks (PneuNets) have emerged as a promising approach for creating flexible and adaptable actuators [20, 21]. PneuNets consist of a series of interconnected air chambers embedded within elastomeric materials that, when pressurized, create predetermined deformation patterns [22]. This architecture enables complex motions while maintaining structural simplicity, making them particularly suitable for rehabilitation devices [23, 24].

The rest of this paper is structured as follows. Section 2 details the structural design and fabrication of soft actuators, including material selection, manufacturing processes, and assembly methods based on hand rehabilitation requirements. Section 3 presents the design optimization of the rotating actuator structure, utilizing Design of Experiments (DoE) and Finite Element Analysis (FEA) methods to evaluate various design parameters. Section 4 provides comprehensive experimental results measuring the actuators' force output and angular displacement, validating the FEA predictions. Finally, Section 5 presents clinical evaluation results demonstrating the glove's effectiveness in rehabilitation training, including range of motion improvements and grasping precision measurements.

2. Materials and Methods

This study employed an integrated approach combining design, optimization, fabrication, and experimental validation to develop a soft actuator rehabilitation glove. Figure 1 presents the overall research methodology framework. The specific details of each part will be presented in the next sections.

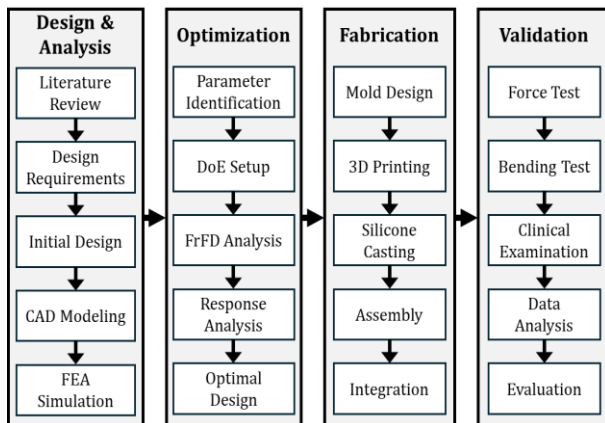


Figure 1: The design process of a wearable glove

2.1. Design and Fabrication of Soft Actuators

2.1.1. System Overview

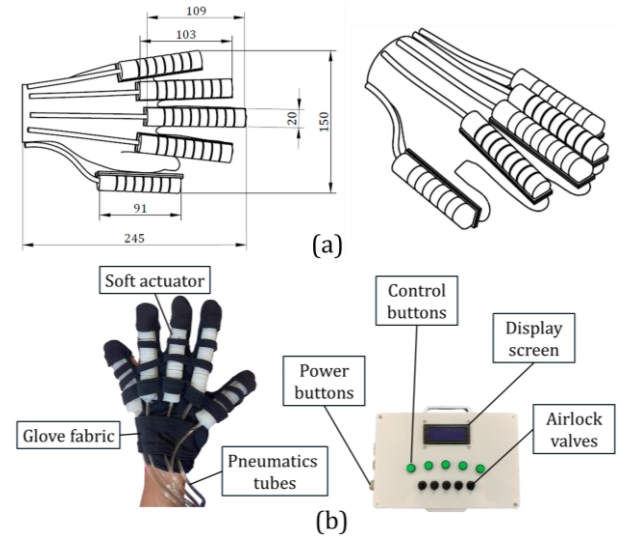


Figure 2: (a) 3D CAD model and (b) physical prototype of the wearable glove

The human hand is capable of flexible movements based on a complex structure consisting of 29 muscles, 19 bones, and 19 joints that allows 22 degrees of freedom for motion. Variations in the biological limits of the structure contribute to the unique motion of each person's hand [25, 26]. Figure 2 shows the 3D CAD model (a) and physical prototype (b) of the actual wearable glove system developed in this study, which consists of the soft actuator-based glove and its control box. The design of the custom developed two-dimensional soft finger actuator is mounted on a fabric-based glove. The dimensions of each finger actuator were determined based on anthropometric data of the Asian population [27], with specific lengths provided in Table 1.

Table 1. Anthropometric measurements of finger lengths in Vietnamese adults [27]

The fingers	Average finger length
Thumb finger	91 mm
Index finger	103 mm
Middle finger	109 mm
Ring finger	103 mm
Little finger	91 mm

The system operates on a 12V power supply and utilizes a PIC16F887A microcontroller to control the pneumatic valve system. The system has a potentiometer to control the pump speed and an integrated pressure sensor to monitor air pressure and provide real time feedback to the microcontroller. The user interacts with the system via an LCD screen that displays various exercise modes. The system incorporates five pneumatic valves for independent control of contraction and

extension movements of each soft finger actuator, with the complete control system architecture shown in Figure 3.

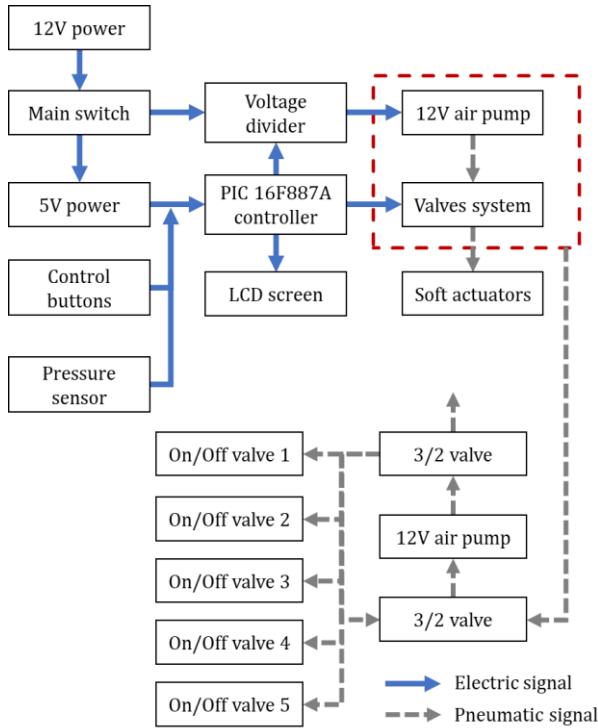


Figure 3: Schematic diagram of the pneumatic control system architecture

The pneumatic circuit features an air pump capable of generating up to 130 kPa pressure to drive the actuators. Two 3/2 directional control valves regulate airflow, with pressurization causing finger contraction and depressurization enabling extension. The system allows precise control of each finger through appropriately adjusted valves. During the operating phase, the pump pressurizes the soft actuator chambers so that the soft actuator achieves different states of contraction and extension with different angles and force intensities.

2.1.2. Design of Bidirectional Soft Pneumatic Actuator

The design of the bidirectional soft pneumatic actuator, as shown in Figure 4, consists of alternating cavities and ribs that provide flexibility for actuation in both directions. The key design parameters include the top wedged angle of the chamber (α), height of the outer beveled edge (d), overall base width (f), wall thickness (t), gap between chambers (e), width of round channels (W), and actuator height (H). These parameters were optimized through comprehensive Finite Element Analysis (FEA) using ANSYS Workbench V19.2 [28], employing a nonlinear structural analysis approach.

The FEA model utilized Dragon Skin 30A silicone properties, represented by an Ogden 3rd order hyperelastic model with material constants $\mu_1 = 3.816 \times 10^{-2}$ MPa, $\mu_2 = 2.524 \times 10^{-2}$ MPa, and $\mu_3 = 4.456 \times 10^{-2}$ MPa (all with $\alpha = 3.417$). The model was discretized using 27,220 SOLID187 tetrahedral elements with refined mesh (1 mm) at critical regions. Boundary conditions included fixed support at the base and internal pressure loading ranging from 0 to 80 kPa, accounting for gravitational effects. The FEA results, shown in Figure 4, demonstrate the actuator's mechanical behavior under operating conditions. The analysis predicted a maximum deformation of 15.827 mm and a maximum reaction force of 4.1247 N at peak pressure, with von Mises stress distributions remaining well below the material's ultimate tensile strength of 3.4474 MPa. The stress patterns reveal optimal load distribution across the chamber walls, validating the design's capability to achieve the required range of motion while maintaining structural integrity. These numerical predictions align well with experimental observations, confirming the effectiveness of the selected geometric parameters and material properties for bidirectional actuation.

These design parameters enable the actuator to achieve bidirectional movement by deforming the structure under pressurization, and they are optimized for flexibility, durability, and control. Each parameter plays a role in balancing strength and elasticity for efficient actuation.

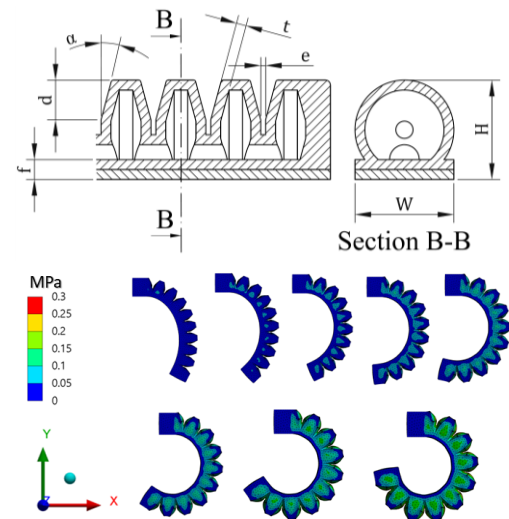


Figure 4: A technical drawing and FEA results (Von Mises stress distribution) of a soft finger actuator

Table 2. Specifications of rehabilitation glove

Characteristic	Specifications
Weight	< 0,5 kg
Speed	10 circle/min
Fingers and thumb curvature	0÷240°
Distal tip force	7,3 N

The soft rehabilitation glove detailed in Table 2 has several key performance characteristics [29]. The glove weighs less than 0.5 kg, making it lightweight and comfortable for the user. It operates at a speed of 10 cycles per minute, which enables consistent movement for rehabilitative purposes. The curvature range for the fingers and thumb is from 0 to 240°, allowing substantial flexibility and range of motion. The distal tip force, which is crucial for gripping tasks, is measured at 7.3 N, providing adequate strength for therapeutic exercises.

2.1.3. Fabrication of Actuators for Soft Gloves

The fabrication process of the soft robotic rehabilitation glove involves several key steps, as indicated in Figure 5. First, a molding design is created to define the shape of the glove's pneumatic chambers. The molds were fabricated using a Peopoly Phenom L MSLA (Masked Stereolithography) 3D printer [30] with a build volume of 345.6 x 194.4 x 400 mm and XY resolution of 0.078 mm (4098 x 2304 pixels). The layer height was set to 0.050 mm for optimal surface finish. The high precision printing enabled production of molds with smooth surfaces, crucial for the quality of the final silicone actuators and consistent chamber dimensions [31]. Silicone material is mixed and poured into these molds to form flexible layers in the glove. The glove is assembled by forming both top and bottom layers, which are bonded together to create airtight chambers. Finally, the glove is fully assembled, including actuators, for rehabilitation purposes.

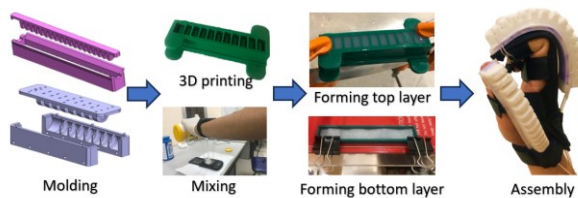


Figure 5: Sequential fabrication methodology of the soft pneumatic rehabilitation glove

The model consists of two primary components: the upper layer with air chambers and the lower base layer, which are separated by a 0.1 mm thick paper layer. Both layers are made from Dragon Skin 30A silicone.

The material used to cast the soft finger actuators includes Dragon Skin 30A silicone, which is characterized by the following Yeoh hyperelastic model parameters: $C_{10} = 0.1202$, $C_{20} = 2.2204 \times 10^{-14}$ and $C_{30} = 0.0018$. Its density is 1080 kg/m³. Additionally, a thick paper layer with a Young's modulus of 6.5 GPa, a Poisson's ratio of 0.2, and a density of 750 kg/m³ is used at the bottom layer of the soft finger actuator.

2.2. Optimization of a Designed Soft Actuator

2.2.1. Screening and Investigation of Design Parameters based on Design of Experiment (DoE)

The DoE technique is essential for optimizing process performance and enhancing product quality. In the context of a soft actuator design, the DoE helps identify which of the six selected parameters significantly affect the minimum inlet pressure, positive force, and negative force generated at the soft fingertip. By systematically varying these parameters and analysing their effects on performance outcomes, engineers can determine the optimal configurations that yield the best results for device operation.

The DoE methodology was implemented to optimize the soft robotic glove, following a systematic approach:

- *Screening*: Six parameters were initially identified: chamber wall thickness (t), number of chambers (n), top wedged angle of the chamber (α), height of the outer beveled edge (d), gap between chambers (e), and bottom layer thickness (f). Each parameter was evaluated at two levels, low (-1) and high (+1), based on the assumption of nearly linear relationships characteristic of first order systems. Higher order nonlinearities necessitate additional levels.
- *Experimental design*: A Fractional Factorial Design was employed to reduce the experimental load, resulting in 32 design points instead of the full factorial 64.
- *Response measurement*: Three primary responses were quantified: FP80 (force at positive 80 kPa), FM60 (force at minus 60 kPa), and BAP60 (required pressure to bend 240 degrees).
- *Effect analysis*: Normal probability plots were utilized to identify significant parameters for each response.
- *Detailed optimization*: Central composite design (CCD) was implemented in two stages, with parameter ranges adjusted based on initial outcomes [32].
- *Visualization and analysis*: Contour plots were generated to illustrate parameter response relationships. The desirability function method facilitates the simultaneous optimization of multiple responses.
- *Validation*: FEA simulations were compared with experimental results to validate the optimized design.
- *Clinical testing*: The optimized design was tested in stroke patients to assess its clinical efficacy.

This DoE approach offers a structured method for thoroughly exploring the design parameters of soft robotic gloves, allowing for efficient identification of key parameters that influence their overall performance. By systematically analyzing these parameters, this approach provides deeper insights into how different design elements interact. This enhances the optimization process by focusing resources on the most impactful variables, reducing the need for exhaustive trial and error testing. Ultimately, this method accelerates the development of high performing soft robotic gloves tailored to specific rehabilitation needs. Each parameter affecting soft actuator formation is considered at low and high levels, as shown in Table 3 below.

The desired outputs for the soft robotic actuator include three key measurements: the force at the tip of the biomechanical soft robotic actuator (BSPA) at a pressure of plus 80 kPa, denoted as FP80; the force at the tip of the BSPA at a pressure of minus 60 kPa, referred to as FM60; and the pressure required to achieve a bending angle of 240 degrees, labelled as BAP60. These abbreviations are crucial for understanding the actuator's performance characteristics.

Table 3. Six design parameters that affect the performance and functions of a soft actuator

Analysis Parameter	Dimension Parameter (mm)	-1 level	+1 level
A	Chamber wall thickness (t)	2	3mm
B	Number of chambers (n)	7	9
C	Top wedged angle of the chamber (α)	5°	20°
D	Height of outer beveled edge (d)	3 mm	9 mm
E	The gap between chambers (e)	1 mm	2 mm
F	Bottom layer thickness (f)	4 mm	5 mm

2.2.2. Dimension Optimization of a Soft Actuator based on Fractional Factorial Design

Fractional Factorial Design (FrFD) is a statistical technique used in experimental design to reduce the number of experiments needed to identify significant parameters affecting a process or system. This approach involves testing only a subset of the possible combinations of parameters, which ultimately saves significant time and resources. If the FrFD technique is not used, the author team will need to conduct 26 simulation experiments to investigate six parameters. Running simulations for each model takes up a significant amount of time. Therefore, by using FrFD in research, we can efficiently and effectively identify significant parameters while minimizing experimental resources.

The design matrix for the $2^{(6-1)}$ FrFD and single replicate response data with the highest possible resolution (VI) and the defining relation $I = ABCDEF$ is obtained from the 32 designs, as shown in Table 4.

Since there is only one replicate of the response variable, the F test is not possible because the error degrees of freedom are zero ($MSE = SSE/0$; division by zero is undefined). A potential solution can be a graphical solution such as a normal probability diagram of effects, a parameter effect estimate, or the sum of squares data.

Table 5 illustrates the quantitative impact of six design parameters (A to F) on three key outputs (FP80, FM60, and BAP60). Parameter A (chamber wall thickness) consistently dominated, contributing 54.44% to FP80, 59.29% to FM60, and 50.82% to BAP60, indicating its crucial role in reducing force and bending pressure. Parameter D (the gap between chambers) is the next significant parameter, particularly influencing FP80 and BAP60, with contributions of 18.60% and 10.32%, respectively. The data emphasize the importance of these two parameters in optimizing the design.

Table 4. The factorial design matrix for soft actuator formation with the defining relation $I = ABCDEF$

Run order	A	B	C	D	E	F	FP80 (N)	FM60 (N)	BAP60 (kPa)
1	-1	-1	-1	-1	-1	-1	4.60226	0.52702	175.374
2	1	-1	-1	-1	-1	1	2.04646	0.24348	78.576
3	-1	1	-1	-1	-1	1	4.39899	0.90159	199.559
4	1	1	-1	-1	-1	-1	2.50813	0.30315	136.029
5	-1	-1	1	-1	-1	1	4.05895	0.44850	139.143
6	1	-1	1	-1	-1	-1	2.27065	0.23816	95.376
7	-1	1	1	-1	-1	-1	4.65884	0.98833	238.552
8	1	1	1	-1	-1	1	1.92933	0.33143	105.165
9	-1	-1	-1	1	-1	1	3.74830	0.51261	135.689
10	1	-1	-1	1	-1	-1	2.00821	0.23815	91.943
11	-1	1	-1	1	-1	-1	4.38274	0.81745	237.007
12	1	1	-1	1	-1	1	1.66383	0.31840	98.708
13	-1	-1	1	1	-1	-1	2.68150	0.91658	126.988
14	1	-1	1	1	-1	1	0.90102	0.21618	58.576

Run order	A	B	C	D	E	F	FP80 (N)	FM60 (N)	BAP60 (kPa)
15	-1	1	1	1	-1	1	1.84211	0.33204	119.869
16	1	1	1	1	-1	-1	0.29821	0.06977	44.99
17	-1	-1	-1	-1	1	1	3.82280	0.62055	140.888
18	1	-1	-1	-1	1	-1	2.16547	0.25285	98.396
19	-1	1	-1	-1	1	-1	4.40933	0.65932	245.767
20	1	1	-1	-1	1	1	1.82924	0.30579	105.504
21	-1	-1	1	-1	1	-1	3.83452	0.95334	162.493
22	1	-1	1	-1	1	1	1.75726	0.25568	75.684
23	-1	1	1	-1	1	1	3.67608	0.83739	185.328
24	1	1	1	-1	1	-1	1.93763	0.26472	126.399
25	-1	-1	-1	1	1	-1	3.71250	1.03835	163.122
26	1	-1	-1	1	1	1	1.46253	0.25974	73.297
27	-1	1	-1	1	1	1	3.44582	0.50769	184.084
28	1	1	-1	1	1	-1	1.68422	0.23548	120.231
29	-1	-1	1	1	1	1	2.07361	0.54540	101.511
30	1	-1	1	1	1	-1	0.98677	0.21111	73.147
31	-1	1	1	1	1	-1	0.94693	0.19416	100.454

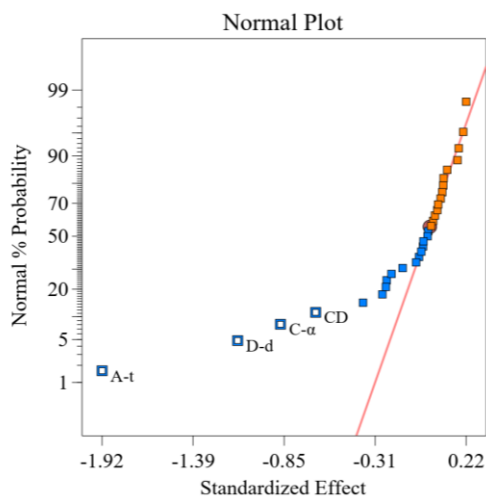


Figure 6: Normal plot of standardized effects of FP80

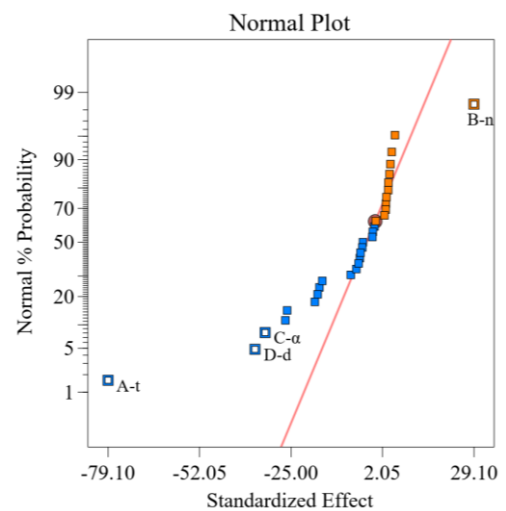


Figure 8: Normal plot of standardized effects of BAP60

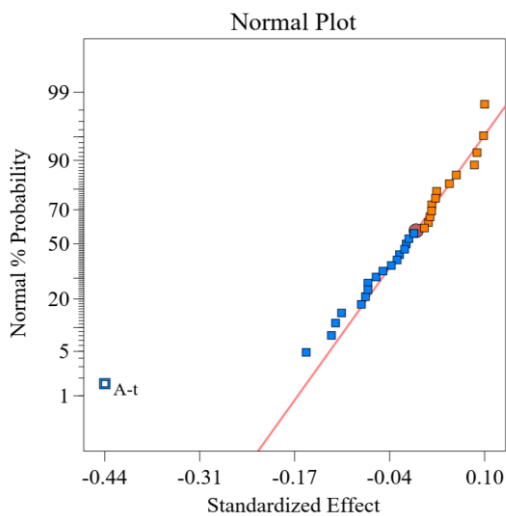


Figure 7: Normal plot of standardized effects of FM60

The standardized effect, sum of squares, and percentage contribution of parameters affecting FM60 in this model are presented in Table 5. Normal probability diagrams of the effects of PF80, FM60, and BAP60, as indicated in Figures 6 to 8, illustrate the standardized effects of various parameters on the three responses (FP80, FM60, and BAP60) of a soft robotic glove. FP80: The number of chambers (B-n) and the chamber top wedge angle (C- α) have significant positive effects. The chamber wall thickness (A-t) and height of the outer beveled edge (D-d) are less influential. FM60: A-t is the dominant parameter, with a strong negative effect. BAP60: Again, B-n has the most significant effect, followed by C- α , whereas A-t has a negative influence. Overall, B-n and C- α are consistently impactful, whereas A-t is mostly negative.

Table 5. Parameter effect estimate and sum of squares

Model term	FP80 (N)			FM60 (N)			BAP60 (kPa)		
	Standardized effect	Sum of squares	Percentage contribution	Standardized effect	Sum of squares	Percentage contribution	Standardized effect	Sum of squares	Percentage contribution
A	-1.92229	29.5615	54.4422	-0.439301	1.54388	59.2916	-79.104	50059.5	50.8202
B	-0.151979	0.184781	0.340304	-0.0239733	0.00459774	0.176573	29.0991	6774.07	6.87701
C	-0.871734	6.07936	11.1961	-0.0569627	0.025958	0.996898	-32.6472	8526.74	8.65632
D	-1.12362	10.1002	18.6011	-0.105673	0.0893338	3.4308	-35.6546	10170	10.3246
E	-0.38532	1.18777	2.18747	-0.0146162	0.00170908	0.0656359	-7.3185	428.484	0.434995
F	-0.271365	0.589113	1.08495	-0.0777555	0.0483673	1.85751	-26.659	5685.62	5.77202

2.2.3. Multiple Response Optimization of Soft Actuator Parameters

Multiple response optimization was performed via response surface methodology with 3 outputs, FP80, FM60, and BAP60 [33]. The four parameters include the chamber wall thickness (t), which ranges from 2 to 3 mm; the number of chambers (n), which ranges from 7 to 9 mm; the top wedged angle of the chamber (α), which ranges from 5 to 20 mm; and the height of the outer beveled edge (d), which ranges from 3 to 9 mm, with three levels: low, medium and high, as indicated in Table 6.

Table 6. Design parameters and their levels for soft actuator optimization

Parameters	Levels (mm)		
	Low (-)	Medium (0)	High (+)
Chamber wall thickness (t)	2	2.5	3
Number of chambers (n)	7	8	9
Top wedged angle of the chamber (α)	5	15	20
Height of outer beveled edge (d)	3	6	9

We used Design Expert V13 software [34] along with the CCD method for optimization and conducted 25 tests with varying combinations of four parameters; an example of a CCD test is shown in Figure 9 [32].

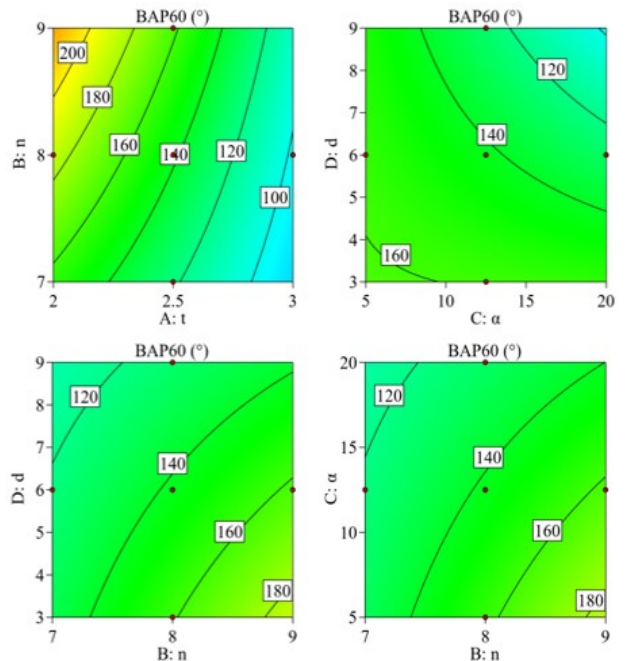


Figure 9: CCD simulation results demonstrating the pressure-angle relationship for BAP60

The results are presented in Table 7. After the first run, the optimal values reached either the highest or lowest limits. Since the true optimum could lie beyond this range, we selected a new range for the second run while keeping the chamber wall thickness at 2 mm. Lowering this parameter risked actuator damage and increased fabrication difficulty, so it was maintained for safety and practicality.

Table 7. Parameters affect soft actuator design

Run	t	n	α	d	FP80 (N)	FN60 (N)	BAP60 (kPa)
1	2	7	5	3	4.602	0.527	175.4
2	3	7	5	3	2.354	0.248	98.8
3	2	9	5	3	4.848	1.003	249.0
4	3	9	5	3	2.508	0.303	136.0
5	2	7	20	3	4.305	0.622	167.7
6	3	7	20	3	2.271	0.238	95.4
7	2	9	20	3	4.659	0.988	238.6
8	3	9	20	3	2.292	0.293	131.0
9	2	7	5	9	4.099	0.735	162.9
10	3	7	5	9	2.008	0.238	91.9
11	2	9	5	9	4.383	0.817	237.0
12	3	9	5	9	2.053	0.296	124.1
13	2	7	20	9	2.682	0.917	127.0
14	3	7	20	9	1.153	0.237	74.2
15	2	9	20	9	2.133	0.308	149.8
16	3	9	20	9	0.298	0.07	45.0
17	2	8	12.5	6	4.070	1.313	183.7
18	3	8	12.5	6	1.920	0.278	102.9
19	2.5	7	12.5	6	2.756	0.321	116.1
20	2.5	9	12.5	6	2.762	0.477	162.1
21	2.5	8	5	6	3.184	0.448	146.5
22	2.5	8	20	6	2.383	0.43	124.5
23	2.5	8	12.5	3	3.369	0.416	149.6
24	2.5	8	12.5	9	2.276	0.405	127.7
25	2.5	8	12.5	6	2.790	0.432	136.0

Table 8 presents the optimization results of the soft actuator formation, comparing three output measures—FP80, FM60, and BAP60—across different finger types. For the force at positive 80 kPa (FP80), the FEA prediction is 5.033 N for the ring/index finger, which is slightly greater than the fitted value of 5.040 N and the experimental results of 4.58 N and 4.49 N, indicating the accuracy of the fitted model.

The values for the little finger/thumb follow a similar pattern, with FEA at 4.896 N, fitted at 4.969 N, and experimental values at 4.47 N and 4.06 N. For the force at negative 60 kPa (FM60), the FEA estimate is 0.982 N for the ring/index finger, with the fitted model closely matching at 0.941 N. Experimental results ranging from 0.70 N to 0.79 N, showing a slight underestimation compared with the FEA model.

The little finger/thumb had similar results, with an FEA of 0.922 N, a fitted value of 0.934 N, and experimental results ranging from 0.73 N to 0.86 N. The bending pressure required to achieve 240 degrees (BAP60) indicates FEA values of 255.1° for the ring/index finger and 208.0° for the little finger/thumb, with the fitted values also closely aligning at 255.1° and 221.7°, respectively. The experimental results suggest higher bending

requirements, notably, 289.7° for the ring/index finger and 196.4° for the little finger/thumb, emphasizing the need for further adjustments in the design. The optimal geometrical parameters indicate a chamber angle (α) of 0° for the ring/index finger and a slight increase to 5.981° for the little finger/thumb, with a chamber thickness (d) of 2.110 mm maintained for both, underscoring its significance in actuator performance. Overall, the optimization process effectively identified key design parameters and demonstrated the robustness of the FEA model compared with the experimental results.

Table 8. Design optimization results of a soft actuator based on FEA and Experiments

Output	Type	Ring/index finger	Little finger/thumb	Middle finger
FP80 (N)	FEA	5.033	4.896	5.203
	Fitted	5.040	4.969	5.182
	Exp	4.58 4.49	4.47 4.06	4.59
FM60 (N)	FEA	0.982	0.922	0.925
	Fitted	0.941	0.934	0.935
	Exp	0.79 0.70	0.86 0.73	0.76
BAP60 (°)	FEA	255.1	208.0	256.0
	Fitted	255.1	221.7	271.7
	Exp	269.6 289.7	209 196.4	305.5
Optimal geometrical parameters	n	9	8	10
	a (°)	0	0	5.981
	D (mm)	2.110	0	0

3. Results and Discussions

3.1. FEA and Experimental Results

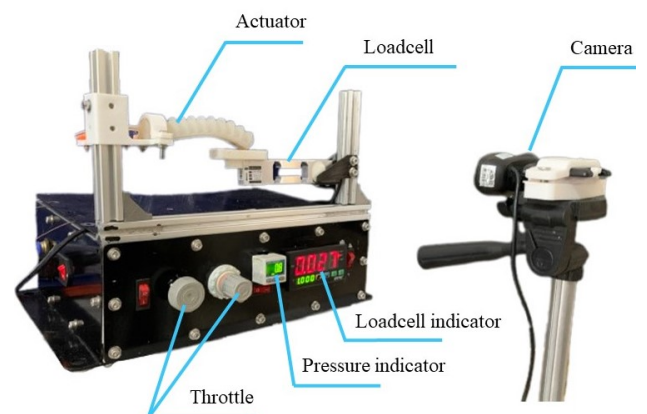


Figure 10: Experimental setup for force characterization

Figure 10 illustrates the experimental setup used for force testing, which includes key components such as the actuator, load cell, pressure indicator, throttle, and camera. The load cell measures the

force, whereas the pressure indicator tracks the internal pressure of the system. The camera records data during the experiment for analysis.

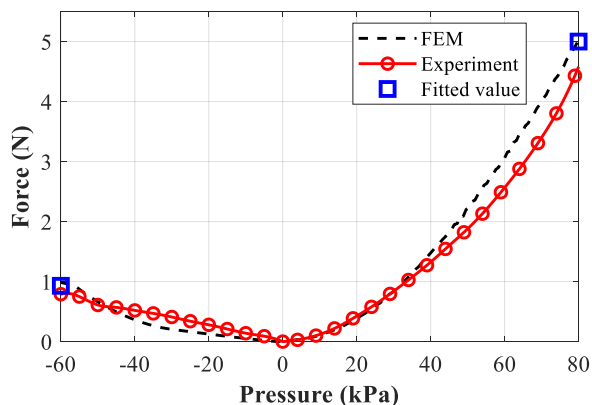


Figure 11: Force-pressure characteristics of the soft actuator

Figures 11 and 12 show the force test and bending test results, respectively, where the pressure varied between -60 kPa and 80 kPa. The force increased from 0 to approximately 5 N, and deformation ranged from 0 to approximately 300 degrees. The experimental data (red circles) closely match the fitted optimization values (blue squares) and the FEA simulation results (dashed black line), particularly at pressures greater than 0 kPa. Below 0 kPa, slight discrepancies can be observed, indicating potential areas for model refinement.

Nonetheless, the overall comparison demonstrates that the FEA simulations and fitted values provide accurate predictions of the system's behavior.

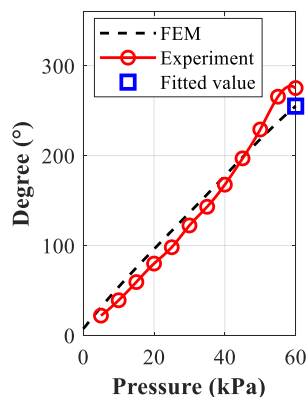


Figure 12: Angular deformation response versus applied pressure

The experimental setup and results for the bending test, as depicted in Figure 12, reveal a clear trend between the applied pressure and the resulting bending angle. The experiment shows that as the pressure increases from 0 to 60 kPa, the bending angle rises almost linearly from 0° to approximately 320°. The experimental data is closely aligned with the fitted value, while the FEA simulation slightly underestimates the bending degree at higher pressures. This highlights the

accuracy of the experimental results, and the optimization fit compared to the simulation model.

3.2. Clinical Evaluation of Wearable Glove for Rehabilitation

The clinical study was conducted at Hospital C, Da Nang City, Vietnam, with the primary objective of quantifying the improvement in finger joint mobility when using the developed soft robotic glove (Figure 13). Eight stroke patients (S1 to S8) with moderate to severe hand impairment participated in the study. The inclusion criteria required participants to have experienced a stroke at least three months prior, with limited hand mobility but sufficient cognitive ability to follow instructions. The study protocol was approved by the hospital's ethics committee, and all participants provided informed consent.



Figure 13: Clinical evaluation protocol implementation at Hospital C, Da Nang, Vietnam

We employed a standardized measurement protocol using a manual goniometer from Baseline® Evaluation Instruments with $\pm 1^\circ$ precision to assess joint angles [35]. Measurements focused on three key joint levels: the Interphalangeal (IP) joint of the thumb, and the Proximal Interphalangeal (PIP) and Distal Interphalangeal (DIP) joints of the fingers. Two trained physical therapists performed the measurements independently to ensure reliability. Joint angles were measured in two conditions: passive movement without the glove (baseline) and assisted movement with the glove activated. For each condition, measurements were taken during both contraction (Figure 14) and extension (Figure 15) movements.

These joints work in coordination to produce the natural grasping and manipulation movements of the hand. Our measurements focused particularly on the contraction and extension angles at each of these joints, as these movements are critical indicators of rehabilitation progress [36].

Statistical analysis was performed using paired t-tests to compare joint angles between baseline and assisted conditions. Results demonstrated significant improvements in range of motion when using the glove, particularly for the PIP and IP joints. The mean improvement in contraction angle was $23.5^\circ \pm 4.2^\circ$ ($p < 0.01$) for PIP joints and $18.7^\circ \pm 3.8^\circ$ ($p < 0.01$) for IP joints. Extension movements showed similar

improvements, with mean increases of $19.8^\circ \pm 3.9^\circ$ ($p < 0.01$) for PIP joints and $15.4^\circ \pm 3.5^\circ$ ($p < 0.01$) for IP joints. DIP joints showed more modest but still significant improvements ($12.3^\circ \pm 2.8^\circ$, $p < 0.05$).

These improvements were particularly notable for patients S1 and S2, who demonstrated the largest gains in functional range of motion [37].

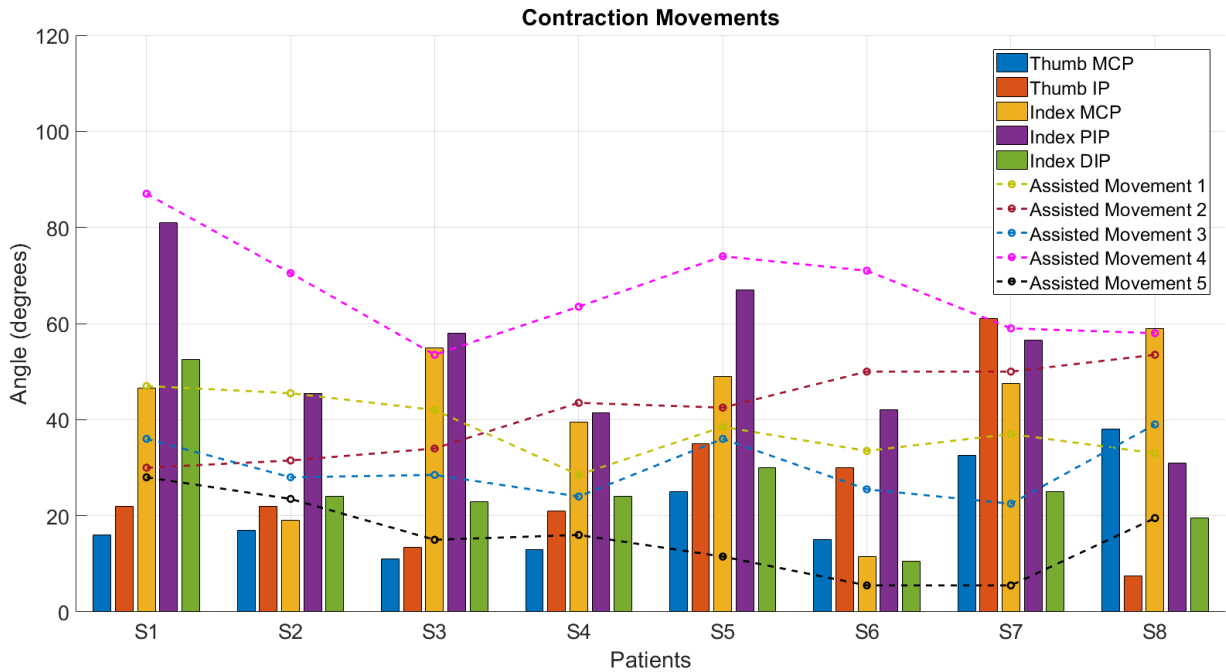


Figure 14: Quantitative analysis of finger joint angles during contraction movements

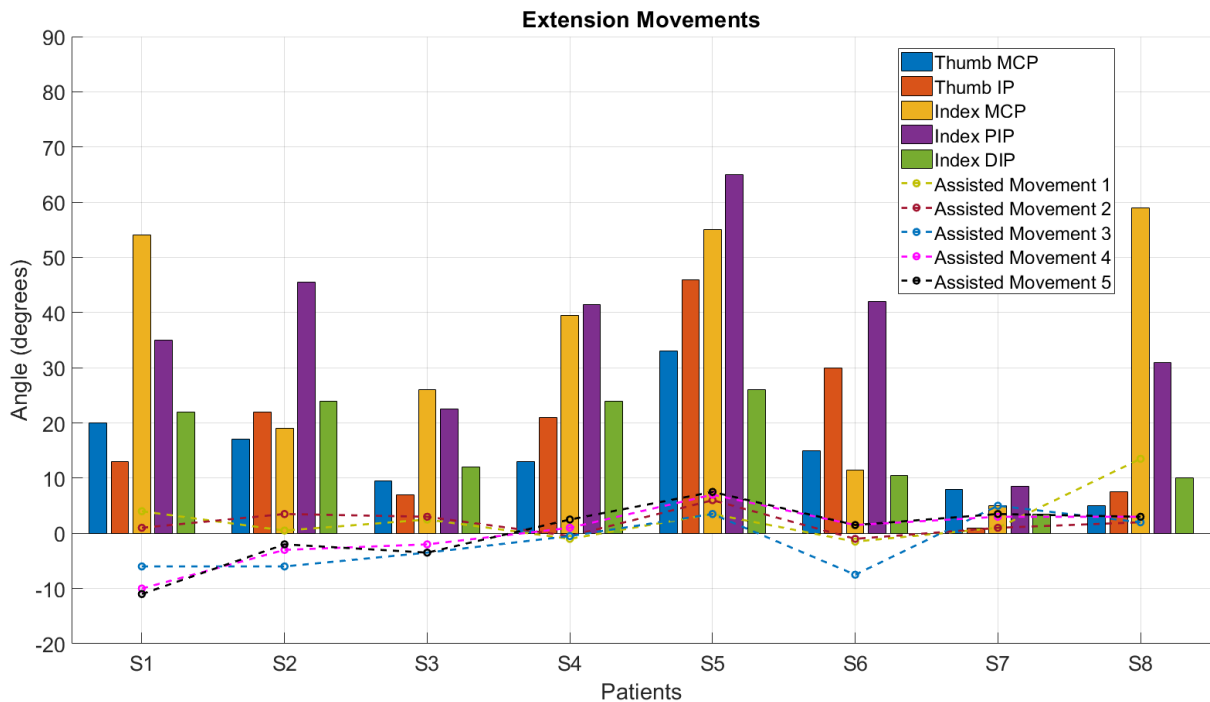


Figure 15: Quantitative analysis of finger joint angles during extension movements

The clinical evaluation revealed that the soft robotic glove effectively assisted finger movements within safe physiological limits. The improvements in joint angles were not only statistically significant but also clinically meaningful, as they exceeded the

minimal clinically important difference of 10° for finger joint motion.

Furthermore, all participants reported comfort during use and no adverse effects were observed during the testing sessions.

4. Conclusions

This research advances the application of PneuNets-based soft actuators for hand rehabilitation devices. Building upon established PneuNet principles, our team developed a bidirectional actuator design that enables both contraction and extension movements. The optimized chamber geometry and material selection resulted in improved force generation and motion control compared to traditional designs. Besides, safety parameters regarding the pressure generated at the joints are also analyzed to ensure user safety. Finally, the actuator is fabricated using elastic Silicone material with a 3D-printed mold casting method.

Experiments on the force generated by the actuator ensure that the force produced is sufficient to help patients perform finger contraction and extension exercises. The experimental results are also compared with FEA analysis to verify the accuracy of the simulation method and prove that this is a reliable method for predicting the behavior of soft actuators. Lastly, the actuator is integrated into a glove and tested with feedback from patients and rehabilitation technicians to evaluate the effectiveness of the solution.

The clinical significance of these improvements was established through multiple criteria. The consistency of improvements across all participants and sustained benefits throughout the study period further validated the device's effectiveness. The results demonstrate that the designed wearable glove provides measurable and significant improvements in hand function, making it a promising tool for stroke rehabilitation. Particularly remarkable was the device's ability to assist both contraction and extension movements effectively, addressing a key challenge in hand rehabilitation.

Acknowledgements

We sincerely thank the staff of the stroke department at Hospital C, Da Nang City, Vietnam, and the Mechatronics Division at The University of Danang for their invaluable support and assistance throughout this project.

References

- [1] Donkor E.S. Stroke in the 21st Century: A Snapshot of the Burden, Epidemiology, and Quality of Life. *Stroke Res Treat.*, 2018:3238165. doi: 10.1155/2018/3238165.
- [2] Mai D.T., Dao X.C., Luong N.K., et al. Current state of stroke care in Vietnam. *Stroke Vasc. Interv. Neurol.* 2022; Vol. 2, no. 2, pp. 1--12. doi: 10.1161/SVIN.121.000331
- [3] Terryn S., Brancart J., Lefeber D., Assche G.V., Vanderborght B. Self-healing soft pneumatic robots. *Sci.Robot.* 2017, vol. 2, doi: 10.1126/scirobotics.aan4268.
- [4] Wege A., Kondak K., Hommel G. Development and Control of a Hand Exoskeleton for Rehabilitation; Proceedings of the IEEE/RSJ International Conference on Intelligent Robots & Systems; Edmonton, AB, Canada. 2-6 August 2005, pp. 3046-3051. doi:10.1109/IROS.2005.1545506.
- [5] Alguacil-Diego I.M., Cuesta-Gómez A., Contreras-González A.F., Pont-Esteban D., Cantalejo-Escobar D., Sánchez-Urán M.Á., Ferre M. Validation of a Hybrid Exoskeleton for Upper Limb Rehabilitation. A Preliminary Study. *Sensors.* 2021, vol. 21:7342. doi: 10.3390/s21217342.
- [6] Terryn S., Brancart J., Lefeber D., Assche G.V., Vanderborght B. Self-healing soft pneumatic robots. *Sci. Robot.* 2017;2 doi: 10.1126/scirobotics.aan4268.
- [7] Lu S., Chen D., Liu C. A 3-D finger motion measurement system via soft strain sensors for hand rehabilitation. *Sens. Actuators A Phys.* 2019, vol. 285, pp. 700-711. doi: 10.1016/j.sna.2018.12.004.
- [8] Chen Y., Tan X., Yan D., Zhang Z., Gong Y. A composite fabric-based soft rehabilitation glove with soft joint for dementia in Parkinson's disease. *IEEE J. Transl. Eng. Health Med.* 2020, vol. 8:1400110. doi: 10.1109/JTEHM.2020.2981926.
- [9] Yi J., Chen X., Wang Z. A three-dimensional-printed soft robotic glove with enhanced ergonomics and force capability. *IEEE Robot. Autom. Lett.* 2017, vol. 3, pp. 242-248. doi: 10.1109/LRA.2017.2737481.
- [10] Ha J., Kim D., Jo S. Use of deep learning for position estimation and control of soft glove; Proceedings of the 2018 18th International Conference on Control, Automation and Systems (ICCAS); PyeongChang, Korea. 17-20 October 2018; pp. 570-574.
- [11] Wang Z., Wang D., Zhang Y., Liu J., Wen L., Xu W., Zhang Y. A three-fingered force feedback glove using fiber-reinforced soft bending actuators. *IEEE Trans. Ind. Electron.* 2019, vol. 67, pp. 7681-7690. doi: 10.1109/TIE.2019.2924860.
- [12] Khalid M.Y., Arif Z.U., Ahmed W. 4D printing: Technological developments in robotics applications. *Sens. Actuators A Phys.* 2022, vol. 343: 113670. doi: 10.1016/j.sna.2022.113670.
- [13] Gerez L., Chen J., Liarokapis M. On the development of adaptive, tendon-driven, wearable exo-gloves for grasping capabilities enhancement. *IEEE Robot. Autom. Lett.* 2019 vol. 4, pp. 422-429. doi: 10.1109/LRA.2019.2890853.
- [14] Panagiotis P., Zheng W. Soft robotic glove for combined assistance and at-home rehabilitation. *Robot. Auton. Syst.* 2015, vol 73, pp. 135-143. doi: 10.1016/j.robot.2014.08.014
- [15] Yap H.K., Khin P.M., Koh T.H. A fully fabric-based bidirectional soft robotic glove for

- assistance and rehabilitation of hand impaired patients. *IEEE Robot. Autom. Lett.* 2017, vol .2, pp. 1383–1390. doi: 10.1109/LRA.2017.2669366.
- [16] Feng M., Yang D., Gu G. High-force fabric-based pneumatic actuators with asymmetric chambers and interference-reinforced structure for soft wearable assistive gloves. *IEEE Robot. Autom. Lett.* 2021, vol. 6, pp. 3105–3111. doi: 10.1109/LRA.2021.3062588.
- [17] Cappello L., Galloway K.C., Sanan S. Exploiting textile mechanical anisotropy for fabric-based pneumatic actuators. *Soft Robot.* 2018, vol 5, pp. :662–674. doi: 10.1089/soro.2017.0076.
- [18] Kim D.H., Heo S.H., Park H.S. Biomimetic finger extension mechanism for soft wearable hand rehabilitation devices; Proceedings of the 2017 International Conference on Rehabilitation Robotics (ICORR); London, UK. 17–20 July 2017; pp. 1326–1330.
- [19] Guo N., Sun Z., Wang X. Simulation analysis for optimal design of pneumatic bellow actuators for soft-robotic glove. *Biocybern. Biomed. Eng.* 2020; vol. 40, pp. 1359–1368. doi: 10.1016/j.bbe.2020.08.002.
- [20] Shepherd R. F., et.,al. Multigait soft robot. Proceedings of the National Academy of Sciences, 2011, Vol 108, No. 51, pp. 20400-20403. doi: 10.1073/pnas.1116564108
- [21] Mosadegh B., et.al. Pneumatic networks for soft robotics that actuate rapidly. *Advanced Functional Materials*, 2014, Vol. 24, no. 15, pp. 2163-2170. doi: 10.1002/adfm.201303288
- [22] Sun Y., Song Y. S., & Paik,J.. Characterization of silicone rubber based soft pneumatic actuators. *IEEE/RSJ International Conference on Intelligent Robots and Systems*, 2013, pp. 4446-4453. doi: 10.1109/IROS.2013.6696995
- [23] Wang T., Ge, L., & Gu G. Programmable design of soft pneumatic actuators with oblique chambers can generate coupled bending and twisting motions. *Sensors and Actuators A: Physical*, 2017, vol. 271, pp. 131-138. doi: 10.1016/j.sna.2018.01.018
- [24] Le H. N., et al., Behavior Analysis of Soft Pneumatic Actuator Gripper by using Image Processing Technology, *2020 IEEE International Conference on Mechatronics and Automation (ICMA)*, Beijing, China, 2020, pp. 1798-1802, doi: 10.1109/ICMA49215.2020.9233746.
- [25] Zhu Y., Gong W., Chu K., Wang X., Hu Z., Su H. A. Novel Wearable Soft Glove for Hand Rehabilitation and Assistive Grasping. *Sensors (Basel)*. 2022 Aug 21;22(16):6294. doi: 10.3390/s22166294.
- [26] Vo N. T. Performance of a Prosthetic Arm Using Mindwave Neurosky Sensor, *8th International Scientific Conference on Applying New Technology in Green Buildings (ATiGB)*, Danang, Vietnam, 2023, pp. 52-56, doi: 10.1109/ATiGB59969.2023.10364464.
- [27] Dunai L., Martin N., Carmen G.E. Human hand anatomy-based prosthetic hand. *Sensors*. 2021; Vol 21, no.1, 137. doi: 10.3390/s21010137
- [28] Ansys (2024). ANSYS Workbench software, Version 19.2. Available at: <https://www.ansys.com> [Accessed: November 15, 2024].
- [29] Polygerinos P., et. al. Towards a soft pneumatic glove for hand rehabilitation. *2013 IEEE/RSJ International Conference on Intelligent Robots and Systems*, Tokyo, Japan, 2013, pp. 1512-1517, doi: 10.1109/IROS.2013.6696549.
- [30] Gul J.Z., et. al. 3D printing for soft robotics - A review. *Sci. Technol. Adv. Mater.* 2018;Vol. 19, pp. 243--262. doi: 10.1080/14686996.2018.1431862.
- [31] Matta C., Tawk C., Rahme P. A review of 3D and 4D printable discontinuous and continuous fibre reinforcement polymers for soft robotics. *Smart Mater. Methods.* 2024; Vol1, pp. 1–56. doi: 10.1080/29963176.2024.2419860.
- [32] Njoku N. C. & Otisi K. S.. Application of Central Composite Design with Design Expert v13 in Process Optimization. *IntechOpen* (2023). doi: 10.5772/intechopen.109704.
- [33] Natarajan, U., Periyanan, P. & Yang, S.H. Multiple-response optimization for micro-endmilling process using response surface methodology. *Int J Adv Manuf Technol*, 2011, Vol. 56, 177–185. doi:10.1007/s00170-011-3156-2.
- [34] Stat-Ease (2024). Design Expert software, Version 13. Available at: <https://www.statease.com/software/design-expert> [Accessed: November 15, 2024].
- [35] Bain G.I., Polites N., Higgs B.G., Heptinstall R.J., McGrath A.M. The functional range of motion of the finger joints. *J Hand Surg Eur.* 2015, vol 40, no.4, pp. 406-411. doi:10.1177/1753193414533754.
- [36] Mansfield PJ, Neumann DA. *Essentials of Kinesiology for the Physical Therapist Assistant*. 3rd ed. Mosby; 2019.
- [37] Sullivan GM, Feinn R. Using Effect Size—or Why the P Value Is Not Enough. *J Grad Med Educ.* 2012; vol 4, no. 3, pp. 279-282. doi:10.4300/JGME-D-12-00156.1.